Arch Virol (2013) 158:1661–1669
DOI 10.1007/s00705-013-1650-6

ORIGINAL ARTICLE

New insight into the structure of RNA in red clover necrotic mosaic virus and the role of divalent cations revealed by small-angle neutron scattering

Stanton L. Martin · Lilin He · Flora Meilleur · Richard H. Guenther · Tim L. Sit · Steven A. Lommel · William T. Heller

Received: 27 November 2012 / Accepted: 24 January 2013 / Published online: 13 March 2013

Abstract Red clover necrotic mosaic virus (RCNMV) is a 36-nm-diameter, T = 3 icosahedral plant virus with a genome that is split between two single-stranded RNA molecules of approximately 3.9 kb and 1.5 kb, as well as a 400-nucleotide degradation product. The structure of the virus capsid and its response to removing Ca^{2+} and Mg^{2+} was previously studied by cryo-electron microscopy (cryo-EM) (Sherman et al. J Virol 80:10395–10406, 2006) but the structure of the RNA was only partially resolved in that study. To better understand the organization of the RNA and conformational changes resulting from the removal of divalent cations, small-angle neutron scattering with contrast variation experiments were performed. The results expand upon the cryo-EM results by clearly showing that virtually all of the RNA is contained in a thin shell that is in contact with the interior domains of the viral capsid protein, and they provide new insight into changes in the RNA packing that result from removal of divalent cations.

S. L. Martin and L. He contributed equally to this work.

Electronic supplementary material The online version of this article (doi:10.1007/s00705-013-1650-6) contains supplementary material, which is available to authorized users.

S. L. Martin · R. H. Guenther · T. L. Sit · S. A. Lommel
Department of Plant Pathology, North Carolina State University, Raleigh, NC 27695, USA

L. He · W. T. Heller
Center for Structural Molecular Biology and Chemical Sciences Division, Oak Ridge National Laboratory, Oak Ridge, TN 37831, USA

L. He · F. Meilleur · W. T. Heller (✉)
Biology and Soft Matter Division, Oak Ridge National Laboratory, Oak Ridge, TN 37831, USA
e-mail: hellerwt@ornl.gov

F. Meilleur
Department of Molecular and Structural Biochemistry, North Carolina State University, Raleigh, NC 27695, USA

Introduction

Red clover necrotic mosaic virus (RCNMV) is the best-characterized member of the plant-exclusive genus *Dianthovirus* [1], family *Tombusviridae*. RCNMV serves as a model system for studying the molecular mechanisms of pathogenesis of plant viruses, and is being investigated for use as a nano-scale cargo vessel in biotechnological applications [2]. Unlike members of other genera in the family *Tombusviridae*, the RCNMV genome is split into two single-stranded positive-sense RNA molecules of 3.9 kb (RNA-1) and 1.5 kb (RNA-2) [3, 4]. RCNMV employs an unusual genome packaging scheme that results in two distinct, but morphologically indistinguishable, virion populations [5]. One population contains a copy of RNA-1 and RNA-2 and at least one copy of a 400-nucleotide degradation product of RNA-1 termed SR1f [6]. The second population contains four copies of RNA-2 [5].

The RCNMV capsid is structurally similar to those of other viruses in the family *Tombusviridae* (such as tomato bushy stunt virus; TBSV) even though the primary amino acid sequences of their capsid proteins (CPs) are only moderately similar [7, 8]. The overall RCNMV capsid structure is a T = 3 quasi-equivalent [9] icosahedron (Fig. 1A) consisting of 180 copies of the 37-kDa CP that exist in three structural conformations, referred to as A, B, and C. A moderate-resolution (8.5 Å) structure of the RCNMV capsid determined by cryo-electron microscopy (cryo-EM) showed an outer diameter of 366 Å and a 174-Å-diameter internal cavity (Fig. 1B) [10].

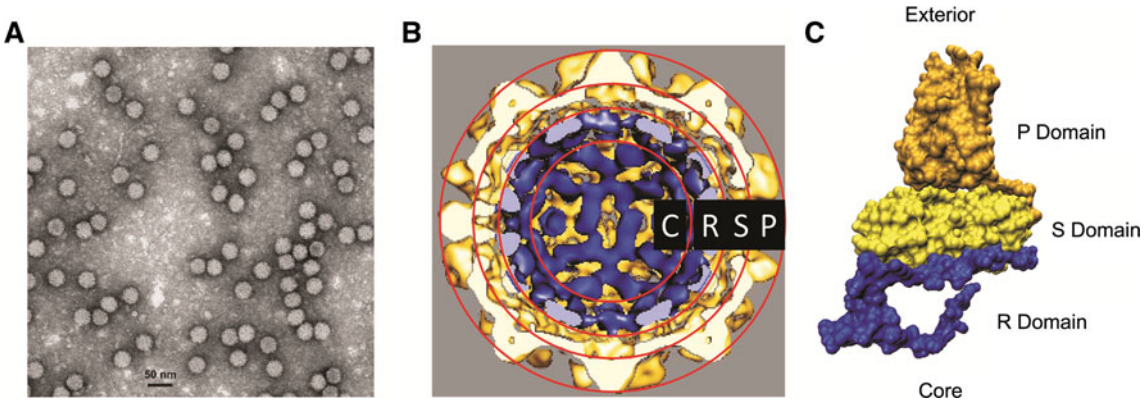

Fig. 1 (**A**) Transmission electron micrograph of negatively stained highly purified (see "Materials and methods") RCNMV virions prepared for SANS measurement. Particles were stained with 2 % (w/v) uranyl acetate. (**B**) Cross section of cryo-EM-based reconstruction of RCNMV [10] with the P, S, R and C shells determined by neutron scattering (red lines). The capsid protein (CP) is shown in yellow (cut away) and dark yellow (exterior). The RNA cage is shown in blue (surface) and purple (cut away). (**C**) Monomer of RCNMV CP in the C conformation showing the P domain (gold), the S domain (yellow) and the R domain (blue) (color figure online)

The RCNMV CP can be divided into three structural domains, termed R for RNA-interacting, S for shell, and P for protruding (Fig. 1B and C). The N-terminal R domain (amino acids 1-46) binds RNA [10] and resides in the interior of the capsid. The S domain (amino acids 47-207) forms the contiguous ~ 30-Å-thick shell that encloses the virion. Pairs of the P domain (amino acids 208-339) tightly associate to create ninety protrusions that extend ~ 37 Å outward from the S shell into the surrounding environment and give the particle its granular appearance when visualized by transmission electron microscopy (Fig. 1A) [11].

The space constraints imposed by the small capsid volume relative to the ~ 5.8 kb of RNA packaged within suggest a high level of condensation of the negatively-charged RNA. The cryo-EM reconstruction revealed an internal RNA cage located between a radius of 87 Å and 117 Å, which is part of the R shell shown in Fig. 1B [10]. Only 35-40 % of the total RNA in the virion was accounted for by the density of the inner cage. It was hypothesized that the remaining RNA unresolved in the cryo-EM reconstruction is loosely packed into the capsid interior. Treatment of RCNMV with chelators of divalent cations induced structural transitions in the capsid [10]. Ca^{2+} removal had no observable effect on the RNA cage within the capsid. Removal of Ca^{2+} and Mg^{2+} resulted in the formation of sixty 11- to 13-Å channels extending through the capsid, but no changes in the RNA-CP or RNA-RNA interactions were observed, in spite of the role of divalent cations in RNA condensation.

To gain new insight into the RNA packaging within RCNMV virions and how the structure responds to the removal of Ca^{2+} and Mg^{2+}, we conducted a series of small-angle neutron scattering (SANS) with contrast variation (CV) experiments on wild-type virions, and SANS experiments on EGTA/EDTA-chelated virions. SANS combined with CV is a powerful non-destructive tool for probing the structures of nucleoprotein complexes in solution [12, 13]. The application of CV makes it possible to analyze structures composed of different materials having different scattering length densities (SLDs). An SLD of a given material is a measure of the strength of the interaction of a neutron with that material. In structural biology, it is possible to leverage the fact that lipids, proteins and nucleic acids have inherently different SLDs. It is possible to greatly vary the SLD of the surrounding solution relative to the components of a complex by mixing H_2O and D_2O thereby leveraging the very different interaction of hydrogen and its isotope deuterium with neutrons. Lipids, proteins and nucleic acids have SLDs that can be 'matched' in ~11 %, ~42 %, and ~65 % D_2O solutions, respectively, thereby eliminating the scattering from that particular component and making it possible to observe other components within an intact structure. SANS with CV has been used to study the structures of numerous icosahedral viruses [14–20]. In this paper, we report the results of SANS CV experiments that allowed us to refine the distribution of the entire volume of RNA within the RCNMV capsid and understand its relationship with the CP. Additional SANS data collected from divalent-cation-depleted virions made it possible to observe conformational changes in the RNA within the core of the virion, expanding our understanding of RCNMV.

Materials and methods

Virus propagation and purification

RCNMV was propagated in *Nicotiana clevelandii* plants as described previously [21]. Virions were isolated from

infected leaves by a differential-centrifugation-based purification process described previously [22] and resuspended in 200 mM sodium acetate buffer, pH 5.2. The initial virus concentration was determined using a NanoDrop 1000 spectrophotometer (Thermo Scientific, Waltham, MA), with an extinction coefficient of 6.46 mg ml^{-1} cm^{-1} at 260 nm [23], and subsequently confirmed using Coomassie Plus Protein Assay Reagent (Pierce Chemical, Rockford, IL). Virion integrity was assayed by transmission electron microscopy of negatively stained samples.

Virus purity

Purified virus preparations were assayed for aggregation using dynamic light scattering (DLS) on a Malvern 1000ES Zetasizer (Malvern Instruments, Worcestershire, UK). To assess the purity of the sample, two electrophoretic assays were conducted to analyze protein and RNA composition separately. A 12 % SDS-PAGE gel was prepared to assay for protein contamination. This gel was loaded with 19.2 μg of RCNMV in both the native and denatured state. Samples were electrophoresed at 150 volts for 50 minutes. The protein bands were visualized by staining with Coomassie blue stain. Virion RNA was extracted by adding 480 μg of diluted virus to 7.5 μl of 20 % SDS. The volume was brought up to 100 μl with Tris-EDTA buffer, pH 7.5, followed by extraction with 100 μl of phenol/chloroform (1:1 v/v), pH 4.3. The viral RNA was ethanol-precipitated and resuspended in 25 μl H_2O. The RNA concentration was determined using a NanoDrop 1000 spectrometer. Viral RNA (0.631 μg) was electrophoresed through a 1 % agarose gel in 1× Tris-acetate EDTA buffer at 90 volts for 60 minutes and visualized by ethidium bromide staining. Gel electrophoresis, dynamic light scattering, and electron microscopy indicated that the virion preparation used for SANS CV consisted of highly purified RCNMV virions.

Small-angle neutron scattering (SANS)

RCNMV was diluted to ~2 mg/ml for all SANS measurements. For wild-type virus, a contrast variation series was made by adding 0.96 μg of the virus, prepared as described above, in an H_2O buffer to 450 μl of mixed buffers composed of 59 %, 63 %, 77 %, 81 % and 90 % D_2O. These D_2O mixtures were employed to ensure that the protein and RNA in the virion were highlighted sufficiently differently in the measurements while maximizing the signal-to-noise ratio. This is done by minimizing the inherently high background that results from neutron scattering from materials possessing a high hydrogen content. By using only D_2O solutions containing greater than 50 % D_2O, the features in the SANS CV data that provide insight into the internal structure of the particle were resolved. Virions treated with a final EGTA concentration of 2 mM or EDTA were mixed with 90 % D_2O only. Samples were measured at room temperature in sealed, 1-mm-path-length quartz cuvettes. The actual D_2O content of the samples was determined using the sample transmission, T, by comparison with pure H_2O and D_2O standards. The neutron absorbance, $\mu = -Ln(T)/d$, where d is the sample thickness, can be related to the fraction of D_2O in the solution, f, through the relation $f = 1 - \left((\mu - \mu_{D_2O})/(\mu_{H_2O} - \mu_{D_2O})\right)$. The measured samples contained 59 %, 63 %, 77 % and 81 % D_2O. The measured D_2O content of the treated samples was 90 %.

The SANS experiments were performed at the HFIR Bio-SANS (CG3), Oak Ridge National Laboratory [24]. The neutron wavelength, λ, was set to 6 Å with a wavelength spread, Δλ/λ, of 0.14. Two sample-to-detector distances, 3 m and 11.3 m, were used to cover a q-range between $q_{\min} = 0.004$ $Å^{-1}$ and $q_{\max} = 0.3$ $Å^{-1}$. The samples and corresponding buffers were collected for 3-5 hours at each detector setting to obtain acceptable counting statistics. The raw 2D data were corrected for the transmission, the detector pixel response and the dark current, which represents the ambient radiation background and electronic noise. The corrected data were azimuthally averaged to produce the 1D profile $I(q)$ vs. q, where $q = 4\pi \sin\theta/\lambda$ and 2θ is the scattering angle. Data were placed on an absolute scale (cm^{-1}) through the use of calibrated standards [25]. The reduced 1D profiles from the two detector distances were merged using methods developed by the National Institute of Standards and Technology [26] and implemented in IGOR Pro 6.1 (WaveMetrics, Lake Oswego, OR). The final reduced data were produced by subtracting the $I(q)$ of the buffer from that of the sample. A constant baseline was also subtracted to account for the displacement of buffer by the virus in the sample.

SANS data modeling

The model fitting was accomplished by approximating the virus as a structure consisting of concentric spherical shells. The intensity profile of the multi-shell model is given by Equation 1.

$$I(q) = \frac{\Phi}{V_p}\left[\sum_{i=1}^{N} \frac{3V_i(\rho_i - \rho_{i+1})j_1(qr_i)}{qr_i}\right]^2 + bkg \qquad (1)$$

The volume fraction of the particles in solution is given by Φ, V_p is the particle volume, V_i and r_i are the volume and radius of the i^{th} concentric sphere, respectively. N is the number of shells used. The function $j_1(x) = (\sin x - x\cos x)/x^2$ is the first spherical Bessel function. All of the contrast variation datasets and the datasets collected at different camera lengths were fit simultaneously for the

shell radii and scattering length densities. The radii were free parameters and were constrained to be identical for all of the CV datasets. The SLDs, also free parameters, were not coupled between datasets from different H_2O/D_2O mixtures. The *bkg* in Equation 1 was also a free parameter for each CV set. The "global fit" non-linear least-squares fitting routines developed by NIST [26] in the IGOR Pro 6.1 software package were used. These routines also accounted for the instrument resolution function. The initial values for the SLDs and thicknesses of the four shells, determined to be the optimal number for fitting the data, were estimated from the RCNMV cryo-EM reconstruction structure [10]. The volume fractions of protein, RNA and solvent in each shell were estimated from the known SLDs of the various components of the virus as a function of D_2O concentration using the relation $\rho = \sum_{i=1}^{3} \phi_i \rho_i$, where ϕ_i and ρ_i are the volume fractions and scattering length densities of the protein, RNA and solvent. A constraint of $\sum_{i=1}^{3} \phi_i = 1$ was also applied.

Additional modeling was performed using the RCNMV capsid structure determined by cryo-EM [10] containing a concentric spherical shell of uniform density to represent the RNA. An atomic-resolution model of the virus capsid was assembled from a homology model based on the 2.9-Å crystal structure of TBSV [7], which was fit to the RCNMV cryo-EM density map [10] after appropriate amino acid substitutions. The resulting model contained a trimer of the three different CP conformations. The complete capsid was generated using the *pdbset* program from the CCP4 program suite [27]. The RNA was modeled as a spherical shell of uniform density with an inner shell radius, *R*, and an outer radius of 131 Å, a value determined from the virion model. The use of a solvent containing core was based on the results of the multi-shell modeling. The calculated volume of the shell was adjusted for the volume occupied by the CP that protruded into the capsid core. The SLD of the RNA shell was calculated from the volume of RNA in the shell at the measured D_2O concentrations. Models were tested for values of *R* ranging from 0 Å to 130 Å in 1-Å intervals. Models having shells with insufficient volume to hold the RNA were not tested. The intensity calculation followed the Monte Carlo method used in ORNL_SAS [28]. The capsid and the spheres were overlaid onto a 1-Å cubic grid, and each grid element was assigned to the capsid, RNA spheres and solvent. The quality of the fit of the model SANS intensity profiles to the measured data were evaluated using the reduced χ^2 parameter used previously [28, 29]. Each model calculation was performed 100 times to determine the average and standard deviation of the χ^2 of each model tested as a function of *R*.

Results

The SANS CV profiles of wild-type RCNMV at various D_2O concentrations are shown in Fig. 2. Guinier analysis for the radius of gyration, R_g, and determination of the distance distribution function *P(r)*, presented in the Supplemental Information, show a primarily monodispersed particle consistent in size with the cryo-EM structure [10]. The SANS profiles were fit using a poly-shell model, which can accurately reproduce the scattering patterns derived from icosahedral virus particles [30]. The solid lines shown in Fig. 2 are the best-fit profiles obtained with the 4-shell model, and the corresponding shells are shown in Fig. 1B overlaid onto the cryo-EM reconstruction [10]. The structural parameters and scattering length densities (SLDs) resulting from the modeling are summarized in Table S2. The volume fractions of protein, RNA and solvent in each shell were estimated from the known SLDs of the various components of the virus as a function of D_2O concentration. The results of this estimation are presented in Table 1. The C shell consists primarily of solvent, although a very small amount of RNA and protein may be present. The volume fractions are on the same order as the uncertainties in the material deconvolution. The R shell is dominated by RNA, as expected, and the S shell consists mostly of the CP shell domain. While the P shell contains some protein, the fitting demonstrates that the bulk of the P shell is occupied by solvent. This result is consistent with the ninety P-domains projecting out from the capsid shell into the solvent (Fig. 1B).

The radial SLD distribution functions, $\rho(r) - \rho_s$, were determined to better understand the distribution of material in the capsid and are presented in Fig. 3. Due to the limited *q*-range of the SANS CV data, the curves below a radius of $\sim$50 Å are unreliable and are not presented. The curves all exhibit a broad feature near a radius of 125 Å. The depth of the feature and the known SLDs of the solvent, CP and RNA indicate that it results from the protein shell. The curves collected at 77 % and 81 % D_2O reveal a second feature at $\sim$ 75 Å in close proximity to the main minimum. This feature results from the RNA in the structure and is visible in these curves because of the improved contrast of the RNA in the high D_2O buffers. The 90 % D_2O concentration provided the greatest contrast for both protein and RNA.

The results of modeling the RNA distribution using a uniform density shell inside an atomic-resolution model of the capsid are shown in Fig. 4. The SANS intensity profiles of one of the best-fitting models, having an inner RNA shell radius, *R*, of 77 Å are shown in Fig. 4A. This structure and a plot of χ^2 as a function of *R* are shown in Fig. 4B, C, respectively. The results of this modeling

approach are in agreement with the 4-shell modeling result. The difference between the radius of the C-shell from the multi-shell model and *R* can be attributed to the different levels of detail used in the two modeling methods, such as the protrusions on the surface of the virion and the R-domain of the CP. These protrusions cannot be represented structurally in the multi-shell modeling approach.

The SANS profiles of RCNMV treated with chelators are shown in Fig. 5. A simpler, two-shell model best fit the chelator-treated data. Additional shells were not justifiable because only a single contrast value (90 % D_2O) was measured. The shell thicknesses, SLD changes and center of mass locations are presented in Table 2. The model fitting indicates that the total diameter of the capsid does not change significantly in response to either treatment. EGTA treatment, which preferentially chelates Ca^{2+}, does not significantly change the thickness of either shell but increases the SLD of both shells, consistent with solvent penetration. The radial distribution functions (Fig. 6) show that the center of mass in both shells has moved inward. In contrast, EDTA treatment, which chelates Ca^{2+} and Mg^{2+}, slightly increases the inner shell thickness while decreasing the outer shell thickness. The SLD of just the outer shell decreases, implying that non-solvent material has entered this layer. The center of mass for both shells has moved inward but the outer shell movement is less pronounced

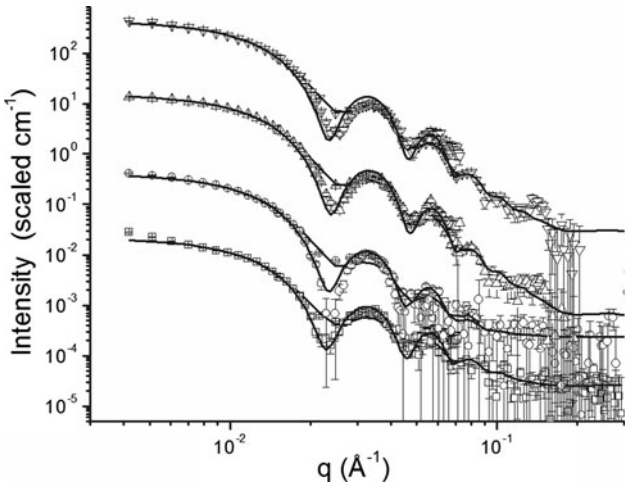

Fig. 2 SANS CV data for RCNMV collected at 59 % D_2O (□), 63 % D_2O (○), 77 % D_2O (Δ) and 81 % D_2O (∇), which have been offset for clarity. The first three points were omitted from the Guinier fitting to reduce the effect of any high-molecular-weight contaminants on the fits. The two sets of SANS CV data collected for each sample at the two different sample-to-detector distances were fit simultaneously using the 4-shell model described in Materials and methods (solid lines). The position of the minima is dictated by the structure of the virion, but the sizes of the oscillations result from the differences between the SLDs of the protein, RNA and solvent. The lower signal-to-noise ratio seen in 59 % D_2O and 63 % D_2O results from the smaller differences between the total SLD of the virion and the solvent than exists in the higher-D_2O-content solvents. Differences are observed in the position of the first minima in the data and fit curves in 77 % D_2O and 81 % D_2O that are not evident in the lower D_2O datasets. Such a difference, which appears large on a log-log plot, may result from using a spherical model to fit an icosahedral particle with an irregular surface and the utilization of a simultaneous fitting of all of the SANS CV data with a single structure

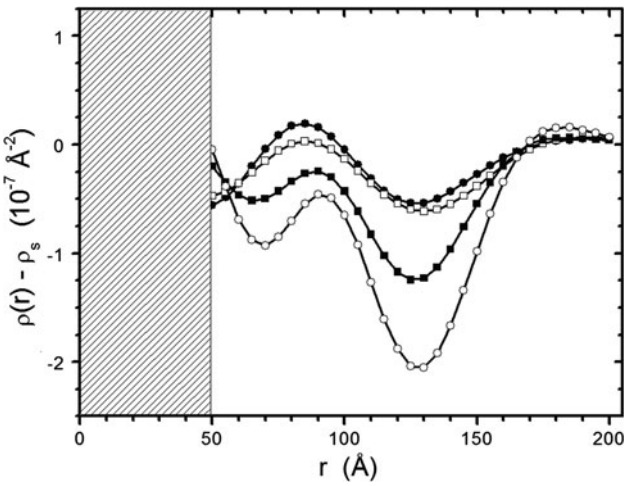

Fig. 3 Radial scattering density distribution functions determined from the SANS CV data collected at 59 % D_2 O (●), 63 % D_2O (□), 77 % D_2O (■) and 81 % D_2O (○). The curves below 50 Å, masked out by the shaded region, are not reliable due to the limited q-range of the instrument. The positions of the features in the curves are dictated by the structure of the virion. The amplitudes of the features result from the differences between the SLDs of the protein, RNA and solvent. The protein, which has a lower SLD than the RNA, can be attributed to the deeper feature in the curves. Measurements above and below the contrast match point of the RNA give rise to the different sign of the smaller feature in the radial scattering length density distribution functions

Table 1 Volume fraction in each shell that is occupied by protein, RNA or solvent determined from the 4-shell fitting of the SANS CV data. The uncertainties in the volume fractions are on the order of a few percent

Shell	Radius (Å)	Volume (× 10^6 Å^3)	Shell composition (%)			Percent of total within shell	
			Protein	RNA	Solvent	Protein	RNA
C	0-88	2.85	3	5	92	1	6
R	88-120	4.38	9	52	39	4	94
S	120-153	7.76	96	0	4	80	0
P	153-182	10.25	13	0	87	14	0

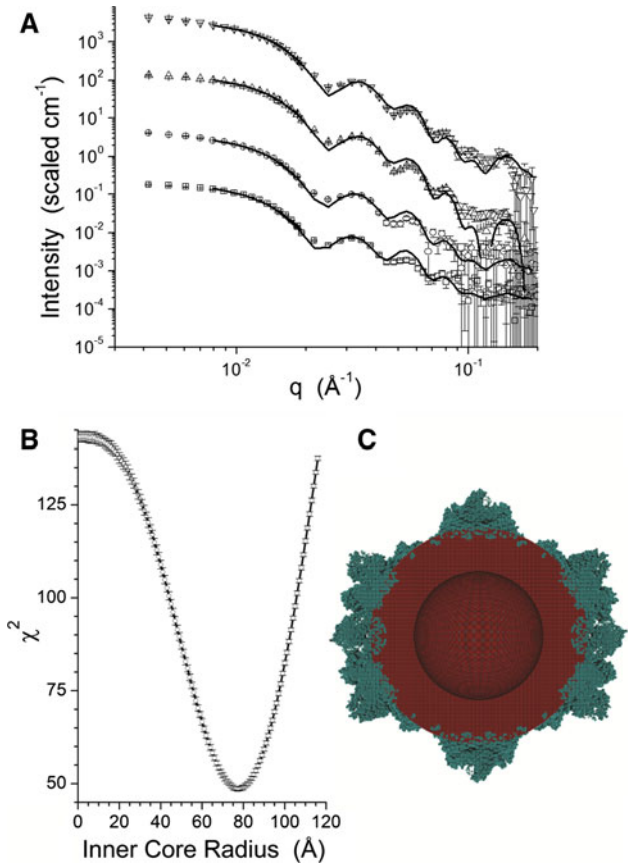

Fig. 4 (**A**) RCNMV SANS CV data collected at 59 % D_2O (□), 63 % D_2O (○), 77 % D_2O (Δ) and 81 % D_2O (▽) with the model intensity profiles (solid lines) determined from the fitting using the model of the CP with the internal shells of RNA. The curves have been offset for clarity, and the number of data points in the overlap region between the two detector distances used was reduced for the model fitting. The first three points were omitted from the fitting to avoid the effect of any high-molecular -weight contaminants on the fitting. (**B**) Chi-squared distribution as a function of the inner radius of the shell and (**C**) the best-fitting structural model, built (as described in "Materials and methods") using a model of the CP threaded into the cryo-EM reconstruction [10]

after EDTA treatment than occurred in response to EGTA treatment (Fig. 7).

Discussion

The results of the RCNMV SANS CV analysis presented highlight the complementary nature of SANS and cryo-EM approaches for the structural investigation of virions. The SANS CV profiles, when combined with the structural information obtained by cryo-EM, made it possible to expand our understanding of the structure of the virion, in particular with respect to the organization of the RNA.

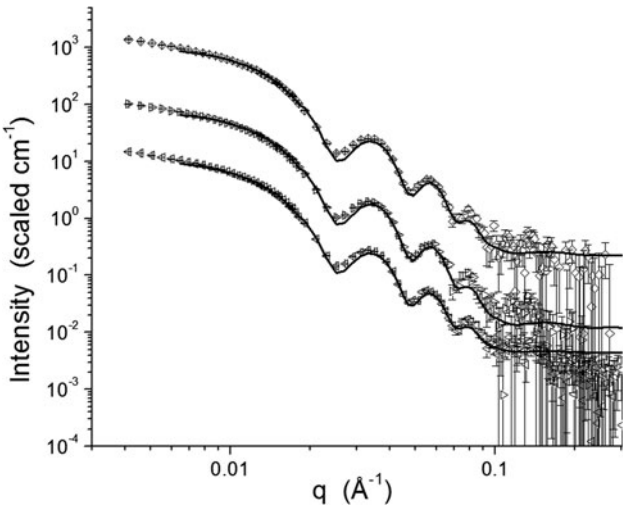

Fig. 5 SANS profiles of RCNMV samples in 90 % D_2O for wild-type particles (◇); EGTA-treated particles (▷); and EDTA-treated particles (◁) with the model intensity profiles (solid lines) determined from the fitting using the 2-shell model. The curves are shifted vertically for clarity

Organization within the virion

The cryo-EM reconstruction of wild-type RCNMV depicted a distinct cage-like distribution of density beginning at a radius of 112 Å and extending to a radius of 122 Å. It was noted that the cage possesses a quasi T = 1 symmetry, while the virion possesses the canonical T = 3 quasi-equivalent symmetry. The volume of highly ordered RNA within this region accounts for 35–40 % of the total RNA known to be packaged within virions. The remaining RNA density is observable; however, the assignment of its location and level of order were insufficient for reconstruction purposes [10]. The SANS results presented here demonstrate that the ordered RNA region actually spans from 88 Å to 122 Å and accounts for ~94 % of the total RNA and 4 % of the total protein (Table 1). The model of the uniform density shell of RNA inside the high-resolution model of the CP is consistent with the results of the simpler modeling of the SANS CV data. The core region contains mostly solvent, along with 1 % protein and the remaining ~6 % RNA.

The SANS results suggest that the two virion populations (RNA-1/RNA-2 and 4 copies of RNA-2 [5]) share a very similar RNA packaging. Significant structural differences between the populations, such as one having a diffusely packed core and the other having a well-defined RNA cage, would be reflected in the densities and radii of the shells. The model best fitting the data would be the single distribution that best represents the population-weighted average scattering from the two particles present in the sample. The quantity of protein found within the

Table 2 Thickness, scattering length density, and center of mass of wild-type and chelated RCNMV samples based on a two-shell SANS model

Sample	Inner shell			Outer shell			Total thickness (Å)
	Thickness (Å)	SLD × 10^{-6} ($Å^{-2}$)	Center of mass (Å)	Thickness (Å)	SLD × 10^{-6} ($Å^{-2}$)	Center of mass (Å)	
WT	105.94 ± 0.61	5.15 ± 0.01	80	54.37 ± 0.78	3.46 ± 0.01	127	160.31
EGTA	104.77 ± 0.67	5.23 ± 0.01	75	55.15 ± 0.86	3.74 ± 0.01	120	159.94
EDTA	106.79 ± 0.58	5.13 ± 0.01	75	53.24 ± 0.75	3.37 ± 0.02	125	160.03

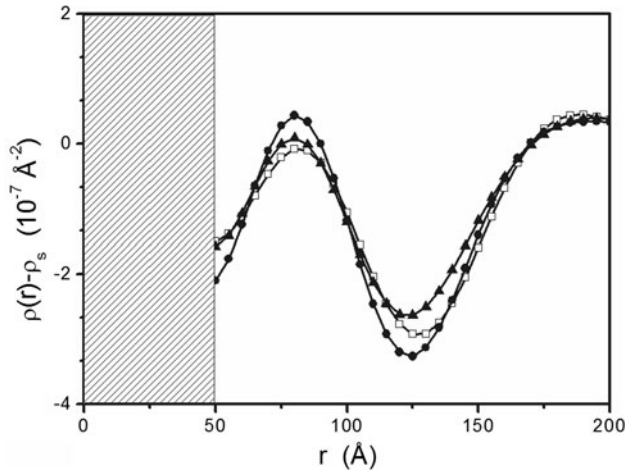

Fig. 6 Radial scattering density distribution functions for non-UV-irradiated wild-type RCNMV (□), EGTA-treated RCNMV (▲), and EDTA-treated RCNMV (●) in 90 % D_2O

primary RNA region in the 4-shell model is consistent with the unresolved 16 residues of the CP, which are positively charged. Molecular studies with brome mosaic virus, another icosahedral RNA plant virus, have indicated that specific N-terminal motifs are involved in the packaging of the RNA genome [31].

A similar internal organization was observed for the related viruses Cucumber necrosis virus (CNV) [32] determined by cryo-EM reconstruction and TBSV by small-angle X-ray scattering and SANS [18]. One major difference between RCNMV and CNV/TBSV is the absence of protein in the inner core of the RCNMV virion. In both CNV and TBSV, a portion of the CP extends into the core of the virion below the RNA layer [18]. The RCNMV CP is 339 residues in length, while the larger CNV and TBSV CPs are 381 and 388 aa residues in length, respectively. The 42- to 49-residue differences are due to longer R domains in both CNV and TBSV, which may partially account for the presence of protein in the inner core of CNV and TBSV.

Changes within the virion after loss of divalent cations

As a means of testing the importance of divalent cations in the RCNMV life cycle (especially the disassembly process), virions were treated with chelators to mimic the environmental changes experienced by virions upon cellular entry. The previous cryo-EM reconstruction of EGTA- or EDTA-treated RCNMV virions produced distinct and stable conformations, which allowed us to assess the interdependency of these cations on the structure of the virion [10]. As was the case in the native virions, the RNA was not fully resolved as a well-ordered region of density in the reconstructions.

Treatment with EGTA results in the removal of almost all of the Ca^{2+} ions and a partial loss of Mg^{2+} ions [10]. SANS analysis of EGTA-treated virions reveals solvent penetration into both shells of the virion (as evidenced by

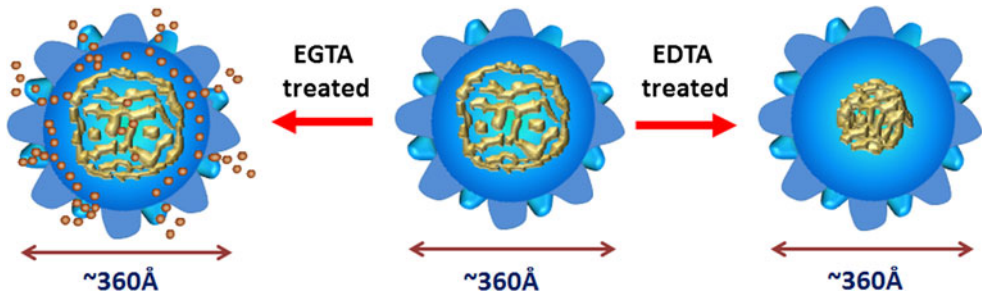

Fig. 7 Schematic depiction of the putative rearrangement of RNA and protein in response to the removal of metallic cations from RCNMV. In wild-type RCNMV (center image), the RNA (gold) is closely associated with the S shell of the RCNMV coat protein. Treatment with EGTA (left image) results in the ingress of solvent (orange spheres) into all shells of the virion and initiates decoupling of the RNA/protein interface. Treatment with EDTA (right image) results in dissociation of the RNA/ protein interface, enabling the RNA to occupy the entire volume of the core of the virion

the increase in SLDs; see Table 2) along with a concomitant inward shift of the centers of mass. This suggests that the changes localized to the outer shell are predominantly due to the loss of surface Ca^{2+} ions associated with the CP while changes to the inner shell are most likely due to the loss of Mg^{2+} ions weakly associated with the RNA that are involved in condensation of the genetic material.

Treatment with EDTA results in the removal of almost all of the Ca^{2+} and Mg^{2+} ions [10]. SANS analysis of EDTA-treated virions reveals that the outer shell displays a decrease in SLD, suggesting either solvent loss or a gain of protein or RNA. The magnitude of the shift in center of mass is between that of the untreated and EGTA-treated virions, suggesting that this shift is likely due to the outward movement of protein. The thickness of the inner shell increased, while the SLD, and therefore the material content, remained virtually unchanged. This change suggests that the RNA had become disordered and likely expanded inwards, as observed by the inward shift in center of mass. This would explain the shift in protein into the outer shell upon disruption of any ordered RNA-protein interactions at the shell interface.

Functional significance of divalent cations in RCNMV pathogenesis

The refined internal structure of RCNMV elucidated by SANS analysis reveals potential conformations of the virion during the early stages of infection. The extracellular concentration of divalent cations is higher than the intracellular one where levels are highly regulated. This cation gradient might be exploited by RCNMV as a potential trigger mechanism to initiate the disassembly process. Removal of divalent cations does not lead to the loss of virion integrity, suggesting that RCNMV does not have an intrinsic disassembly mechanism mediated by ionic changes, as has been proposed for cowpea chlorotic mosaic virus (CCMV) [33]. Instead, the loss of Ca^{2+} and then Mg^{2+} leads to (i) solvent ingress and (ii) the formation of pores through the protein capsid. This provides the opportunity for bidirectional movement. Previously, it was speculated that these pores might serve as a conduit for RNA egress [10]. Based on the inward movement of RNA and outward movement of protein observed in the present SANS analysis, this scenario seems less likely. The RNA becomes disordered upon removal of divalent cations. This leads to the disruption of the RNA-protein complex and the movement of the N-terminal CP residues. This observation supports an alternative hypothesis for the significance of these rearrangements: the N-termini of the CP become surface accessible, potentially traversing the pores. This temporal surface presentation of the N-termini may be a required step in the disassembly process mediated by host processes, as has been proposed for CNV [34, 35].

Acknowledgements This research was supported by the Laboratory Directed Research and Development Program of Oak Ridge National Laboratory (ORNL). The research at ORNL's Center for Structural Molecular Biology (FWP ERKP291) was supported by the U.S. Department of Energy's Office of Biological and Environmental Research. Work at HFIR was sponsored by the Scientific User Facilities Division, Office of Basic Energy Sciences, U.S. Department of Energy. Oak Ridge National Laboratory is managed by UT-Battelle, LLC for the U.S. Department of Energy under contract No. DO-AC05-00OR22725. This manuscript has been authored by UT-Battelle, LLC, under Contract No. DE-AC05-00OR22725 with the U.S. Department of Energy. The United States Government retains, and the publisher, by accepting the article for publication, acknowledges that the United States Government retains a non-exclusive, paid-up, irrevocable, world-wide license to publish or reproduce the published form of this manuscript, or allow others to do so, for United States Government purposes.

References

1. Musil M, Gallo J (1982) Serotypes of red-clover necrotic mosaic-virus.1. Characterization of 3 serotypes. Acta Virol 26(6):497–501
2. Loo L, Guenther RH, Lommel SA, Franzen S (2008) Infusion of dye molecules into red clover necrotic mosaic virus. Chem Commun 1:88–90. doi:10.1039/b714748a
3. Gould AR, Francki RIB, Hatta T, Hollings M (1981) The bipartite genome of red-clover necrotic mosaic-virus. Virology 108(2):499–506. doi:10.1016/0042-6822(81)90457-8
4. Hiruki C (1987) The Dianthoviruses—a distinct group of isometric plant-viruses with bipartite genome. Adv Virus Res 33:257–300. doi:10.1016/s0065-3527(08)60320-6
5. Basnayake VR, Sit TL, Lommel SA (2006) The genomic RNA packaging scheme of red clover necrotic mosaic virus. Virology 345(2):532–539. doi:10.1016/j.virol.2005.10.017
6. Iwakawa HO, Mizumoto H, Nagano H, Imoto Y, Takigawa K, Sarawaneeyaruk S, Kaido M, Mise K, Okuno T (2008) A viral noncoding RNA generated by cis-element-mediated protection against 5′- > 3′ RNA decay represses both cap-independent and cap-dependent Translation. J Virol 82(20):10162–10174. doi:10.1128/jvi.01027-08
7. Harrison SC, Olson AJ, Schutt CE, Winkler FK, Bricogne G (1978) Tomato bushy stunt virus at 2.9-Å resolution. Nature 276(5686):368–373. doi:10.1038/276368a0
8. Olson AJ, Bricogne G, Harrison SC (1983) Structure of tomato bushy stunt virus.4. The virus particle at 2.9 Å resolution. J Mol Biol 171(1):61–93. doi:10.1016/s0022-2836(83)80314-3
9. Caspar DLD, Klug A (1962) Physical principles in construction of regular viruses. Cold Spring Harbor Symp Quant Biol 27:1–24
10. Sherman MB, Guenther RH, Tama F, Sit TL, Brooks CL, Mikhailov AM, Orlova EV, Baker TS, Lommel SA (2006) Removal of divalent cations induces structural transitions in red clover necrotic mosaic virus, revealing a potential mechanism for RNA release. J Virol 80(21):10395–10406. doi:10.1128/jvi.01137-06
11. Xiong Z, Lommel SA (1989) The complete nucleotide-sequence and genome organization of red-clover necrotic mosaic-virus rna-1. Virology 171(2):543–554. doi:10.1016/0042-6822(89)90624-7
12. Jacrot B (1976) Study of biological structures by neutron-scattering from solution. Rep Prog Phys 39(10):911–953. doi:10.1088/0034-4885/39/10/001

13. Heller WT (2010) Small-angle neutron scattering and contrast variation: a powerful combination for studying biological structures. Acta Crystallogr Sect D-Biol Crystallogr 66:1213–1217. doi:10.1107/s0907444910017658
14. Jacrot B, Pfeiffer P, Witz J (1976) Structure of a spherical plant-virus (bromegrass mosaic-virus) established by neutron-diffraction. Philos Trans R Soc Lond Ser B-Biol Sci 276(943):109–112. doi:10.1098/rstb.1976.0101
15. Cusack S, Ruigrok RWH, Krygsman PCJ, Mellema JE (1985) Structure and composition of influenza-virus—a small-angle neutron-scattering study. J Mol Biol 186(3):565–582. doi:10.1016/0022-2836(85)90131-7
16. Inoue H, Timmins PA (1985) The structure of rice dwarf virus determined by small-angle neutron-scattering measurements. Virology 147(1):214–216. doi:10.1016/0042-6822(85)90242-9
17. Witz J, Timmins PA, Adrian M (1993) Organization of turnip yellow mosaic-virus investigated by neutron small-angle scattering at 80-K—an intermediate state preceding decapsidation of the virion. Proteins 17(3):223–231. doi:10.1002/prot.340170302
18. Aramayo R, Merigoux C, Larquet E, Bron P, Perez J, Dumas C, Vachette P, Boisset N (2005) Divalent ion-dependent swelling of tomato bushy stunt virus: a multi-approach study. Biochim Biophys Acta-Gen Subj 1724(3):345–354. doi:10.1016/j.bbagen.2005.05.020
19. He LL, Piper A, Meilleur F, Myles DAA, Hernandez R, Brown DT, Heller WT (2010) The structure of sindbis virus produced from vertebrate and invertebrate hosts as determined by small-angle neutron scattering. J Virol 84(10):5270–5276. doi:10.1128/jvi.00044-10
20. He LL, Piper A, Meilleur F, Hernandez R, Heller WT, Brown DT (2012) Conformational changes in sindbis virus induced by decreased pH are revealed by small-angle neutron scattering. J Virol 86(4):1982–1987. doi:10.1128/jvi.06569-11
21. Xiong ZG, Lommel SA (1991) Red-clover necrotic mosaic-virus infectious transcripts synthesized invitro. Virology 182(1):388–392. doi:10.1016/0042-6822(91)90687-7
22. Martin SL, Guenther RH, Sit TL, Swartz PD, Meilleur F, Lommel SA, Rose RB (2010) Crystallization and preliminary X-ray diffraction analysis of red clover necrotic mosaic virus. Acta Crystallogr F-Struct Biol Cryst Commun 66:1458–1462. doi:10.1107/s1744309110032483
23. Lommel SA (1983) Ph.D. Dissertation. University of California, Berkeley, Berkeley, CA
24. Lynn GW, Heller W, Urban V, Wignall GD, Weiss K, Myles DAA (2006) Bio-SANS—a dedicated facility for neutron structural biology at oak ridge national laboratory. Physica B 385–86:880–882. doi:10.1016/j.physb.2006.05.133
25. Wignall GD, Bates FS (1987) Absolute calibration of small-angle neutron-scattering data. J Appl Crystallogr 20:28–40. doi:10.1107/s0021889887087181
26. Kline SR (2006) Reduction and analysis of SANS and USANS data using IGOR Pro. J Appl Crystallogr 39:895–900. doi:10.1107/s0021889806035059
27. Bailey S (1994) The CCP4 suite-programs for protein crystallography. Acta Crystallogr Sect D-Biol Crystallogr 50:760–763
28. Tjioe E, Heller WT (2007) ORNL_SAS: software for calculation of small-angle scattering intensities of proteins and protein complexes. J Appl Crystallogr 40:782–785. doi:10.1107/s00218898070242 0x
29. Heller WT (2006) ELLSTAT: shape modeling for solution small-angle scattering of proteins and protein complexes with automated statistical characterization. J Appl Crystallogr 39:671–675. doi:10.1107/s0021889806029591
30. Li X, Shew CY, He LL, Meilleur F, Myles DAA, Liu E, Zhang Y, Smith GS, Herwig KW, Pynn R, Chen WR (2011) Scattering functions of Platonic solids. J Appl Crystallogr 44:545–557. doi:10.1107/s0021889811011691
31. Choi YG, Rao ALN (2000) Molecular studies on bromovirus capsid protein VII. Selective packaging of BMV RNA4 by specific N-terminal arginine residues. Virology 275(1):207–217. doi:10.1006/viro.2000.0513
32. Katpally U, Kakani K, Reade R, Dryden K, Rochon D, Smith TJ (2007) Structures of T = 1 and T = 3 particles of cucumber necrosis virus: Evidence of internal scaffolding. J Mol Biol 365(2):502–512. doi:10.1016/j.jmb.2006.09.060
33. Lavelle L, Michel JP, Gingery M (2007) The disassembly, reassembly and stability of CCMV protein capsids. J Virol Methods 146(1–2):311–316. doi:10.1016/j.jviromet.2007.07.020
34. Hui E, Rochon D (2006) Evaluation of the roles of specific regions of the cucumber necrosis virus coat protein arm in particle accumulation and fungus transmission. J Virol 80(12):5968–5975. doi:10.1128/jvi.20485-05
35. Xiang Y, Kakani K, Reade R, Hui E, Rochon D (2006) A 38-amino-acid sequence encompassing the arm domain of the cucumber necrosis virus coat protein functions as a chloroplast transit peptide in infected plants. J Virol 80(16):7952–7964. doi:10.1128/jvi.00153-06